PTB–INRIM comparison of novel digital impedance bridges with graphene impedance quantum standards

OPEN ACCESS
IOP Publishing | Bureau International des Poids et Mesures Metrologia
Metrologia **59** (2022) 065001 (11pp) https://doi.org/10.1088/1681-7575/ac9187

PTB–INRIM comparison of novel digital impedance bridges with graphene impedance quantum standards

Martina Marzano[1,*], Yaowaret Pimsut[2,3], Mattias Kruskopf[2], Yefei Yin[2], Marco Kraus[2], Vincenzo D'Elia[1], Luca Callegaro[1], Massimo Ortolano[1,4], Stephan Bauer[2] and Ralf Behr[2]

[1] Istituto Nazionale di Ricerca Metrologica, Strada delle Cacce, 91, 10135 Torino, Italy
[2] Physikalisch-Technische Bundesanstalt, Bundesallee 100, 38116 Braunschweig, Germany
[3] National Institue of Metrology (Thailand), Pathum Thani 12120, Thailand
[4] Politecnico di Torino, Corso Duca degli Abruzzi 24, 10129 Torino, Italy

E-mail: m.marzano@inrim.it

Received 18 May 2022, revised 8 September 2022
Accepted for publication 13 September 2022
Published 3 October 2022

Abstract

This paper describes an onsite comparison of two different digital impedance bridges when performing measurements on a quantum Hall resistance standard with the purpose of realizing the SI unit of capacitance, the farad. In the EMPIR Joint Research Project 18SIB07 GIQS, *graphene impedance quantum standards*, the Physikalisch-Technische Bundesanstalt (PTB), Germany, developed a Josephson impedance bridge, and the Istituto Nazionale di Ricerca Metrologica (INRIM) and the Politecnico di Torino (POLITO), Italy, developed an electronic digital impedance bridge. The former is based on Josephson waveform generators and the latter on an electronic waveform synthesizer. The INRIM–POLITO impedance bridge was moved to PTB and the two bridges were compared by measuring both temperature-controlled standards and a graphene AC quantized Hall resistance (QHR) standard. The uncertainties for the calibration of 10 nF capacitance standards at 1233 Hz are within 1×10^{-8} for the PTB's bridge and around 1×10^{-7} for the INRIM–POLITO's bridge. The comparison mutually validates the two bridges within the combined uncertainty. The result confirms that digital impedance bridges allow the realization of the SI farad from the QHR with uncertainties comparable with the best calibration capabilities of the BIPM and the major National Metrology Institutes.

Keywords: impedance metrology, quantized Hall resistance standards, impedance bridges, graphene, Josephson arbitrary waveform synthesizers

(Some figures may appear in colour only in the online journal)

1. Introduction

Since the 2018 revision to the International System of Units (SI) [1], the units of impedance, ohm Ω, farad F and henry H, can be realized by using a quantized Hall resistance (QHR) standard, either in DC (DCQHR standard) or AC (ACQHR standard) [1, appendix 2], [2–4].

In the DC approach, a DCQHR standard is employed to calibrate a resistance standard with an accurately known AC–DC transfer ratio [5–7], allowing its DC value to be transferred to the working frequency of interest.

In the AC approach, an ACQHR standard is employed to directly calibrate a resistance or a capacitance standard

* Author to whom any correspondence should be addressed.

at the frequency of interest. Before the introduction of digital technologies, this operation could be performed only by means of transformer-ratio bridges, where an impedance ratio is compared with a voltage or current ratio generated by a transformer [8, 9]. A resistance standard can be calibrated by a transformer-ratio bridge against a single ACQHR standard, but the calibration of a capacitance standard requires a quadrature bridge with two ACQHR standards [10]. This is a complex apparatus achieving the highest measurement accuracy, but whose implementation and operation is beyond the capabilities of most national metrology institutes. In recent years, however, impedance bridges based on polyphase digital signal synthesizers and capable of measuring impedance ratios across the whole complex plane have emerged as measuring systems suitable for primary impedance metrology [11–22]. In these *fully-digital* impedance bridges, an impedance ratio is determined by a voltage ratio generated by either an electronic polyphase synthesizer or two Josephson arbitrary waveform synthesizers (JAWS). Impedance bridges of this kind, compared to traditional transformer-ratio bridges, are simpler to implement and operate, making them suitable and affordable by a broader range of laboratories, from national metrology institutes to calibration laboratories.

For the implementation of QHR standards, gallium arsenide (GaAs) devices have been the workhorses of resistance and impedance metrology for about thirty years, but graphene devices have recently proved to be a viable alternative, allowing the realization of the quantum Hall effect at lower magnetic field and higher temperature with respect to those needed with GaAs devices [23–27].

Within the framework of the EMPIR joint research project 18SIB07 GIQS, *graphene impedance quantum standards* [28], the Physikalisch-Technische Bundesanstalt (PTB), Germany, developed a four-terminal-pair Josephson digital impedance bridge, and the Istituto Nazionale di Ricerca Metrologica (INRIM) and the Politecnico di Torino (POLITO), Italy, developed a four-terminal-pair electronic digital impedance bridge to enable an efficient traceability of impedance quantities to a graphene ACQHR. To assess the performance of these novel impedance bridges in the realization of the unit farad with a mutual validation, the INRIM–POLITO impedance bridge was moved to PTB. A short summary reporting the concept of this assessment was presented in [29] and this paper presents the full results of the comparison.

Sections 2 and 3 briefly describe the two impedance bridges. Section 4 describes the ACQHR employed in the comparison. Section 5 describes the temperature-controlled resistance and capacitance standards also employed in the comparison. Finally, section 6 reports and discusses the experimental results.

In the following, all relevant impedances are defined as four-terminal-pair (4TP) impedances [30], and the impedance of the ACQHR standard is defined by the well-known triple-connection scheme [31]. The terms *terminal pair* and *port* will be considered as equivalent and used interchangeably.

2. The PTB Josephson impedance bridge

2.1. General description

The Josephson impedance bridge is designed to perform: (i) ratio measurements of like impedances (resistor to resistor $R:R$ or capacitor to capacitor $C:C$); (ii) quadrature measurements of unlike impedances (resistor to capacitor $R:C$); and (iii) ratio measurements of an impedance standard to a graphene ACQHR standard. Details about all components of the bridge, the Josephson system and most of the balancing procedure can be found in [22]. Since the measurement of type (iii) is presented in detail in [22], here we focus on the description of measurement types (i) and (ii). The ratio measurement of equal impedances is typically performed in a frequency range from 53 Hz to 50 kHz with rms signal amplitudes up to 100 mV. Measurement frequencies below 50 Hz are possible too, but this would need a different set of detection transformers. In fact, the system is operated at 53 Hz as its lowest frequency to avoid the harmonics of the power line frequency (50 Hz). Also higher operating frequencies should be possible but have not been tested yet.

Figure 1 shows a schematic diagram of the bridge. The two Josephson junction arrays (marked with X) consist of 9000 and 12 000 junctions and are immersed in liquid helium. The impedance standards used in this work are described in section 5. Two active equalizers are added in different network meshes of the impedance bridge to ensure current equalization: one between the output of *JAWS1* and the detection transformer D_{HP1} and one between the low potential terminal of Z_2 (LP2) and the ultra-low noise AC amplifier before the detector D_2.

2.2. Balancing procedure

The procedure starts with the adjustment of the currents in the high potential arms. For this purpose, two sources S_1 and S_2 are used to inject currents I_{HC1} and I_{HC2} at the high current ports HC1 and HC2, respectively. The amplitude and phase of I_{HP1} and I_{HP2} are changed until the detector readings of D_{HP1} and D_{HP2} are minimized. Next, the Kelvin balance will be carried out by adjusting amplitude and phase of the source S_{K} to minimize the difference between the detector readings at LP1 and LP2. The main balance is defined by detector readings U_{D1} and U_{D2} and its real and imaginary parts are minimized by tuning the amplitude and phase of voltage U_2. The adequate phase setting of detector D_1 and D_2 were deduced from a 100 μV V^{-1} jump of the real part U_1 which is also used to determine the sensitivity coefficients for the ratio measurements. In an iterative process, the amplitude and phase of U_2 are adjusted until the detector readings U_{D1} and U_{D2} are close to zero.

The impedance ratio is calculated as

$$\frac{Z_2}{Z_1} = \frac{U_2}{U_1}\left[1 + \frac{1}{2}\left(\frac{U_{\mathrm{D1}}}{S_1} + \frac{U_{\mathrm{D2}}}{S_2}\right) + \frac{1}{2}\left(\frac{U_{\mathrm{D1}}}{S_{\mathrm{K1}}} - \frac{U_{\mathrm{D2}}}{S_{\mathrm{K2}}}\right)\right], \quad (1)$$

where S_1 and S_2 are the sensitivity coefficients of the bridge for the Z_1 and Z_2 connection networks. S_{K1} and S_{K2} denote coefficient terms for the Kelvin injection networks. For the case of a perfectly balanced bridge, U_{D1} and U_{D2} equal zero

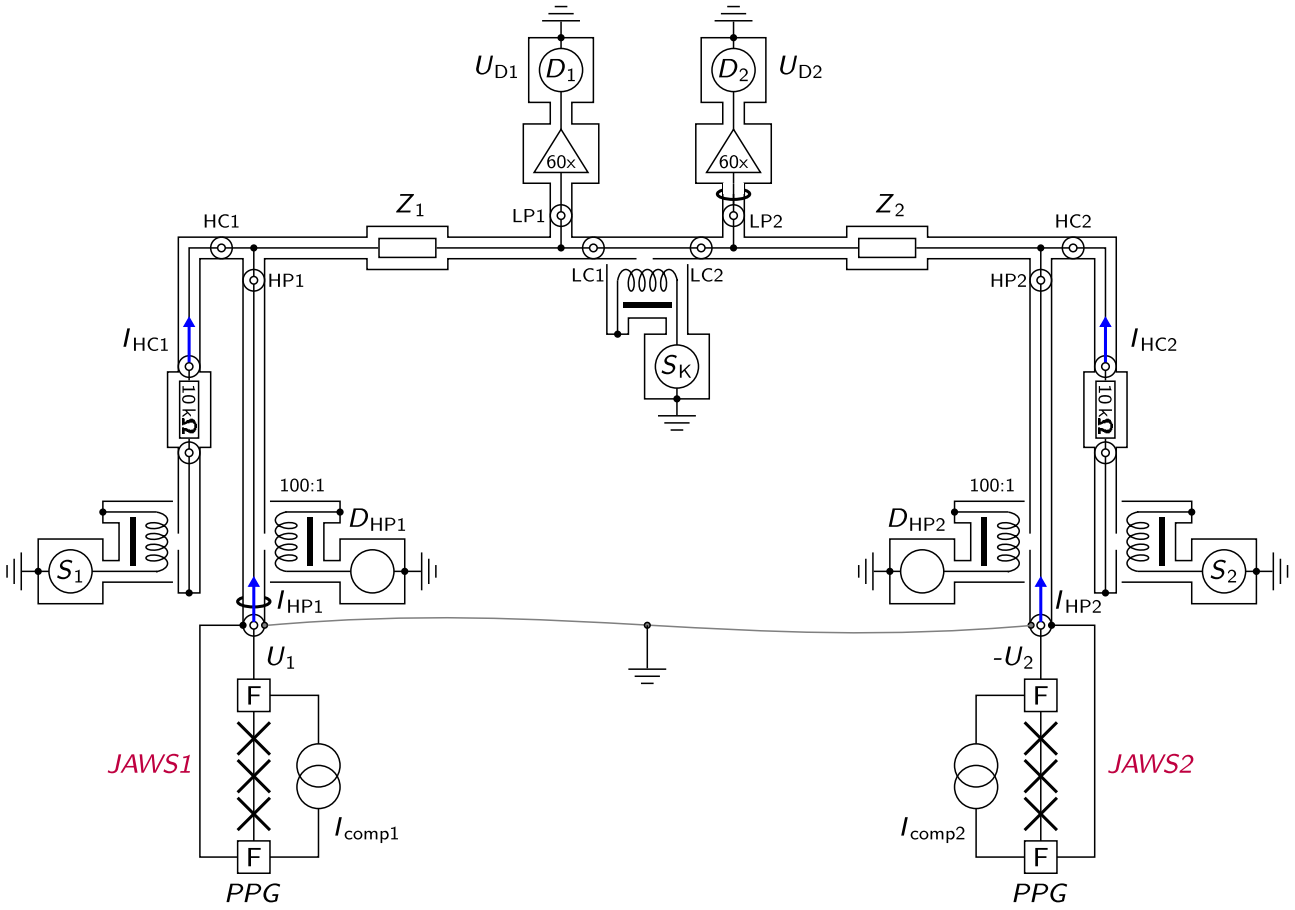

Figure 1. Schematic diagram of PTB's 4TP Josephson impedance bridge setup comparing two impedance standards Z_1 and Z_2. The high potential ports HP1 and HP2 of both impedance standards are defined by voltages from *JAWS1* and *JAWS2*, respectively. On-chip low-pass filters are labeled with 'F'. The injected currents I_{HC1} and I_{HC2} at the high current ports HC1 and HC2 are adjusted until the readings of detection transformers D_{HP1} and D_{HP2} in the high potential arms are close to zero. The Kelvin source S_K is connected at the low current ports LC1 and LC2 to balance the output voltages at low potential ports LP1 and LP2. The amplified voltages U_{D1} and U_{D2} are measured by detectors D_1 and D_2.

and the impedance ratio deduced from (1) is simply given by

$$\frac{Z_2}{Z_1} = \frac{U_2}{U_1}. \tag{2}$$

To compensate systematic errors in the bridge setup (e.g., connecting cables, imperfect grounding), the ratios were measured in *forward* (F) and *reverse* (R) configurations. The forward configuration is defined by applying U_1 to Z_1 and U_2 to Z_2. The forward ratio is detected as $(Z_2/Z_1)_F$. The reverse configuration is achieved when voltages U_2 to Z_1 and U_1 to Z_2 are applied. The complete bridge is rebalanced after changing the applied potentials as described above. The reverse ratio is detected as $(Z_2/Z_1)_R$. The final ratio is given by the geometric mean of the forward and reverse measurements

$$\frac{Z_2}{Z_1} = \sqrt{\left(\frac{Z_2}{Z_1}\right)_F \left(\frac{Z_2}{Z_1}\right)_R}. \tag{3}$$

In addition to the aforementioned impedance ratio measurements, the 4TP Josephson impedance bridge can also be used to directly compare impedance standards to a graphene ACQHR standard. A detailed description of this device can be found in section 4. The schematic diagram of the measurement setup can be found in [22]. Due to the unique features of the QHR no Kelvin injection is needed. Therefore, the balancing procedure reduces to the optimization of the currents in the high potential arms and of the main balance. The impedance is now given by

$$\frac{Z_2}{R_H} = \frac{U_2}{U_1} + \frac{U_D}{U_1} S, \tag{4}$$

where S is the sensitivity coefficient. Further information on this setup and measurement results can be found in [22].

2.3. Uncertainty considerations and contributing components

The measurement models used in the evaluation of the uncertainty for an impedance ratio measurement and for the comparison of an impedance standard to the graphene ACQHR standard are presented in (a) and (b) below:

(a) Uncertainty of an impedance ratio measurement. The ratio W of the impedances can be calculated from (1), and the mathematical model for the uncertainty evaluation is determined as

$$W + \Delta W = (U_{\text{ratio}} + \Delta U_{\text{JAWS}} + \Delta U_{\text{cable}}) \times [1 + (M + \Delta M) + (K + \Delta K)], \quad (5)$$

with $W = Z_1/Z_2$, $U_{\text{ratio}} = U_1/U_2$, $M = (U_{\text{D1}}/S_1 + U_{\text{D2}}/S_2)/2$, $K = (U_{\text{D1}}/S_{\text{K1}} - U_{\text{D2}}/S_{\text{K2}})/2$ and ΔW is the uncertainty of the ratio value. ΔU_{JAWS}, ΔU_{cable}, ΔM and ΔK are approximated uncertainties related to the components which are used to calculate the ratio.

(b) Uncertainty for comparing an impedance standard to the graphene ACQHR. The ratio W_{QHR} of an impedance to the QHR is calculated from (4), and the mathematical model for the uncertainty evaluation is determined as

$$W_{\text{QHR}} + \Delta W_{\text{QHR}} = U_{\text{ratio}} + \Delta U_{\text{JAWS}} + \Delta U_{\text{cable}} + D + \Delta D, \quad (6)$$

with $W_{\text{QHR}} = R_{\text{QHR}}/Z_2$, $U_{\text{ratio}} = U_1/U_2$, $D = (U_{\text{D}}/U_1)S$ and ΔW_{QHR} is the uncertainty of the impedance to the QHR ratio. ΔU_{JAWS}, ΔU_{cable} and ΔD are approximated uncertainties related to the components which are used to calculate the ratio.

The individual uncertainty components are:

- Bridge resolution. The resolution of the bridge is given by the Type A uncertainty. It is limited by the combined noise level at the detection point, which is mainly caused by the noise from the impedance standards (e.g. Johnson noise of the impedance standard) and the input noise of the pre-amplifier (0.6 nV $\sqrt{\text{Hz}}^{-1}$ [32]). The resolution of the bridge is calculated from an Allan variance analysis with a typical measurement time of 2 min. For a $C:C$ measurement at 1233 Hz, this yields a Type A uncertainty of 3 nV V^{-1}.
- JAWS voltage (ΔU_{JAWS}). We estimate an uncertainty contribution of the JAWS voltage ratio due to possible crosstalk between the Josephson arrays and the inductance of the arrays correlated with an improper phase adjustment between compensation currents and pulses. The crosstalk component is strongly reduced by encapsulating both Josephson arrays in special designed copper boxes [15]. At 1233 Hz an error of less than 1 nV V^{-1} is deduced. Due to the inductance of the Josephson arrays, typically in the range from (15.5 to 18.5) nH for the arrays used in this work, an error contribution must be considered. This error is linearly increasing with current and frequency [33–35]. Overney *et al* [20] have shown that the error is strongly suppressed in the geometric mean of a forward and reverse ratio. To make a conservative estimate, we claim for the JAWS voltages in the kHz-range a combined uncertainty within the limit of 5 nV V^{-1}.
- Cable corrections (ΔU_{cable}). The cables used in the setup affect the measured value in two ways. First, the magnitudes of the JAWS voltages at the impedance inputs differ from the JAWS on-chip voltages depending on the cable length and connecting components between the JAWS arrays and impedance standards. However, this error is compensated by forward and reverse measurements [20]. The concerned cable correction is the effect of connecting cables on the 4TP definition. Here, cables on the high potential ports and low current ports are taken in account. The uncertainty is deduced from the detected change in a balanced bridge state when an additional cable of known length is added to the aforementioned locations inside the bridge.
- Bridge deviation (ΔM or ΔD). For the impedance ratio, the bridge deviation error contributes to the term ΔM of (5). The error emerges mainly from an improper balance of currents in the high potential arms which affects the detected voltage values at the low potential ports. For the ratio of an impedance and a QHR standard, the bridge deviation error is affected in the already described manner and appears in the term ΔD of (6). The values for ΔM or ΔD are determined when the currents in the high potential ports (I_{HP}) deliberately unoptimized excess the criteria values of the bridge balance.
- Kelvin network (ΔK). The error of the Kelvin network affects the output values U_{D1} and U_{D2}. The error is determined when deliberately an improper current from the Kelvin network is injected to the bridge.

3. The INRIM–POLITO electronic digital impedance bridge

Figure 2 reports the schematic diagram of the INRIM–POLITO 4TP electronic digital impedance bridge. A detailed description of a preliminary version of this bridge and its operating details can be found in [21]. A brief summary of the bridge's main components, the changes with respect to the preliminary version of the bridge network and to the balance procedure, and the uncertainty considerations are herewith described.

3.1. Bridge components

The 4TP impedances under comparison are Z_1, with ports HC1, HP1, LC1 and LP1, and Z_2, with ports HC2, HP2, LC2 and LP2. When either Z_1 or Z_2 is an ACQHR standard, the device is connected to the bridge by means of a cryogenic coaxial probe [36] implementing the triple-connection scheme. In the following, we shall assume that Z_1 is a calibrated impedance and Z_2 is a possibly uncalibrated one.

The bridge determines the ratio $W = Z_1/Z_2$ and is designed to yield the best accuracy when $|W| \approx 1$, for either $R:R$, $C:C$ or $R:C$ comparisons ($W \approx 1$ in the first two cases, and $W \approx \pm j$ in the last one).

The bridge is mainly composed of an electronic polyphase digital sinusoidal waveform synthesizer [37] operating at frequency f, whose channels can be individually adjusted in magnitude and phase, and of a phase-sensitive detector D used to detect the bridge balance (Stanford Research SR830 lock-in amplifier). The bridge operating frequency is from 20 Hz to 20 kHz, defined by the specification of the digital synthesizer.

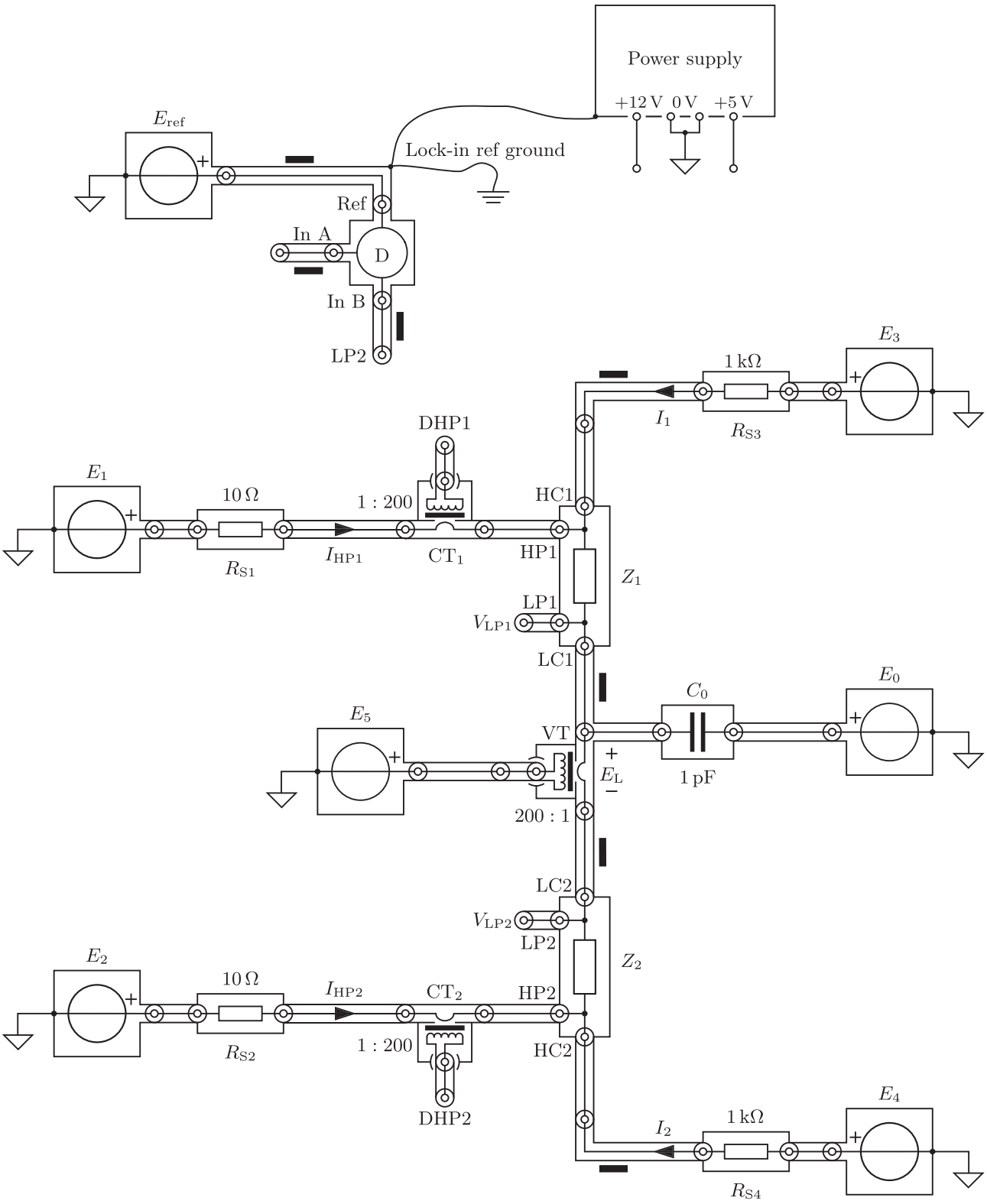

Figure 2. Coaxial schematic diagram of the INRIM–POLITO electronic digital impedance bridge. The black rectangles represent coaxial equalizers.

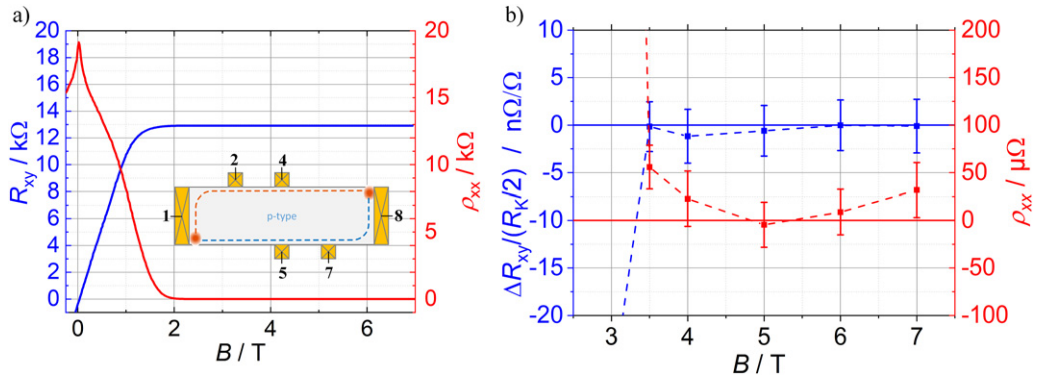

Figure 3. Magnetotransport measurements of the graphene QHR device. (a) In the overview measurement, the plateau starts around $B = 2$ T. The obtained transport properties are p-type (holes) charge carrier density of $p = 5.5 \times 10^{10}$ cm^{-2} and a mobility of $\mu = 5900$ cm^2 V^{-1} s^{-1}. (b) High accuracy measurements with a CCC-bridge verify the accurate quantization at dc at magnetic flux densities between $B = 3.5$ T and $B = 7$ T. Since the minimum of the longitudinal resistivity of $\rho_{xx} = (-4 \pm 24)$ μΩ is identified at $B = 5$ T, this point was chosen as the optimal point of operation also for the AC measurements. The contact pairs for the measurements of ρ_{xx} and R_{xy} are 5 & 7, and 4 & 5, respectively. The current is applied between contacts 1 and 8. The measurements are performed at a current of ≈38 μA at a temperature of 4.2 K.

3.2. Bridge network

The detector's input A is manually switched across the ports DHP1, DHP2 and LP1; its input B is instead permanently connected to the port LP2. When D is connected to DHP1 or DHP2, it measures the voltages V_{DHP1} and V_{DHP2} which, through the 1 : 200 feedthrough transformers CT_1 and CT_2, are proportional to I_{HP1} and I_{HP2}, respectively. When D is connected to LP1 it can measure either just V_{LP1} or the difference $V_{\mathrm{LP1}} - V_{\mathrm{LP2}}$ in the A − B differential input mode. This is a significant update with respect to the bridge network described in [21, figure 2], which improves the balance. The number of current equalizers has been changed accordingly.

3.3. Balancing procedure

The bridge is balanced and the impedances properly defined as 4TP impedances when $V_{\mathrm{LP1}} = 0$, $V_{\mathrm{LP1}} - V_{\mathrm{LP2}} = 0$ and $V_{\mathrm{DHP1}} = V_{\mathrm{DHP2}} = 0$. The details of the balancing procedure are reported in [21]. To cancel the non-linearity error of the synthesizer, a measurement is actually composed of two successive balances [12, 38], as described also in section 2.2 for the PTB bridge: in the forward (F) configuration, the impedances are connected as in figure 2; in the reverse (R) configuration, the two impedances are exchanged at the ports HP1, HC1, HP2 and HC2, further imposing that the digital samples used to generate E_1 and E_2 are exactly the same as those of the forward configuration, at most shifted in time [21]. This constraint can indeed be fulfilled only when $|W| \approx 1$. In a series of repeated measurements, the balances are performed in the sequence FRRFFR…to partially cancel any first-order drift [39, 40] of the generated voltages due to temperature changes.

3.4. Uncertainty considerations and contributing components

The bridge main uncertainty components are described in [21, 41]. In addition to those, the following terms have also been considered in the present work:

- The cable correction $\Delta W^{\mathrm{cable}}$ [8]. This is given by

$$\frac{\Delta W^{\mathrm{cable}}}{W} \approx -\frac{1}{2}\Big(Z_{\mathrm{HP2}}Y_{\mathrm{HP2}} + Z_{\mathrm{LC2}}Y_{\mathrm{LC2}} - Z_{\mathrm{HP1}}Y_{\mathrm{HP1}} - Z_{\mathrm{LC1}}Y_{\mathrm{LC1}} + Z_{\mathrm{HP}}^{\mathrm{QHR}}Y_{\mathrm{HP}}^{\mathrm{QHR}} + Z_{\mathrm{LC}}^{\mathrm{QHR}}Y_{\mathrm{LC}}^{\mathrm{QHR}}\Big), \quad (7)$$

  where Z_{HP2}, Y_{HP2}, Z_{LC2}, Y_{LC2}, Z_{HP1}, Y_{LP1}, Z_{LC1} and Y_{LC1} are the equivalent cable parameters—series impedance and parallel admittance—of the cables connecting the bridge to the ports HP and LC of Z_2 and Z_1, respectively; and where $Z_{\mathrm{HP}}^{\mathrm{QHR}}$, $Y_{\mathrm{HP}}^{\mathrm{QHR}}$, $Z_{\mathrm{LC}}^{\mathrm{QHR}}$ and $Y_{\mathrm{LC}}^{\mathrm{QHR}}$ are the equivalent cable parameters of the HP and LC cables of the triple connection when Z_1 is an ACQHR (these parameters are zero for normal impedances).
- The asymmetry error ΔW^{asym}. The synthesizer is programmed to ensure that the samples synthesizing the waveforms of E_1 and E_2 in the forward and reverse configurations are exactly the same, so that, ideally, for the source readings it holds $E_{1\mathrm{R}}^{\mathrm{read}} = \pm E_{1\mathrm{F}}^{\mathrm{read}}$ and $E_{2\mathrm{R}}^{\mathrm{read}} = E_{2\mathrm{F}}^{\mathrm{read}}$ (plus for like impedances and minus for quadrature impedances). In practice however, when exchanging the standards, asymmetries in the two configurations can lead to different voltages at the high potential ports (e.g. because the current equalizers are not perfect or because of temperature changes between the forward and reverse configurations), thus causing a measurement error.

4. The AC QHR standard

The graphene material and the lithographic fabrication of the Hall device were realized in the cleanroom facility of the PTB Braunschweig as described in the literature [42]. The device is 400 μm wide and about 1600 μm long. Compared to the standard DC design with typically eight contacts, the number of contacts was reduced to the minimum of six contacts (see

inset of figure 3(a)) required for the triple connection in the AC measurement. This design was chosen to minimize capacitive coupling between the device and its surrounding.

The graphene device is installed into a TO-8 carrier with an AC specific design that applies a double-shield composed of electrodes above and below the device that are split into two parts in the center of the device [43]. The double shield design may be used to tune the capacitive losses in the device by applying voltages to the left side of the shield [44]. However, in this study the left side was kept floating while the right side was shorted to the low potential side of the Hall bar. The mounted device was then placed in a 7 T liquid helium-cooled cryomagnetic system located next to the Josephson impedance bridge. All six connection lines are coaxial cables with a characteristic impedance of 75 Ω. From the DC magnetotransport measurements performed in the Josephson impedance lab (figure 3(a)), the charge carrier density was found to be of p-type at a relatively low level of $p = 5.5 \times 10^{10}$ cm^{-2}. The charge carrier mobility was on the level of $\mu = 5900$ cm^2 V^{-1} s^{-1}. Despite the low charge carrier density, the device was found to be accurately quantized at a magnetic flux density of $B = 5$ T at a temperature of 4.2 K when it was measured with the cryogenic current comparator (CCC) DC resistance bridge. These measurements were performed using about 30 m of cable between the CCC bridge and the graphene device. At this point of operation, ρ_{xx} was found to be zero within the uncertainties ($\rho_{xx} = (-4 \pm 24)$ μΩ). The measurements of ΔR_{xy} in figure 3(b) were performed by direct comparison of the QHR against a 100 Ω primary resistance standard in the CCC bridge at the contact pair 4 and 5. The longitudinal resistivity $\rho_{xx} = R_{45} - R_{47}$ was determined from the resulting difference of two Hall measurements with the CCC.

5. Temperature-controlled impedance standards

The 4TP impedance standards (beside the ACQHR standard) used in this work were developed by PTB and by INRIM. The PTB standards are two 10 nF capacitance standards and one 12.9 kΩ resistance standard (the value is about 15 μΩ Ω^{-1} off from the DC value of the QHR standard). The two 10 nF capacitance standards are composed of four 10 nF chip capacitors selected from a batch of commercial standard components arranged in a series/parallel connection. The time-dependent drifts of both capacitance standards are less than −2 nF F^{-1} per day. The drift was evaluated by measurements which are traceable to PTB's ACQHR devices over a period of more than 2 years. The resistance standard is implemented by four commercially available resistance chips which are connected in series. The time-dependent drift of this standard is approximately −2.26 nΩ Ω^{-1} per day. The standard was measured frequently over almost 3 years with a CCC. The frequency dependence was determined with an IVD bridge against a well-known reference resistance to be 0.145 μΩ Ω^{-1} kHz^{-1}. The small time-dependent drifts of all three standards do not need to be considered for the comparison of both impedance bridges since measurements are typically done within one working day. Each standard is installed into a thick-walled aluminum housing. They are hermetically encapsulated by sealing a copper lid with indium. Such a sealed and stiff housing ensures a pressure dependence of the impedance standards which is below our measurement capabilities. All standards are located in the same two-stage thermostat developed and setup at PTB. The operating temperature of the thermostat is 30 °C and the stability is in the mK range. The thermostat is equipped with a backup battery to provide a stable temperature even during transportation to the different calibration laboratories inside PTB.

The INRIM standard is a 12.9 kΩ resistance standard and is implemented by a commercially available oil-filled resistor (Vishay H series). The standard is thermostated and the operating temperature of the thermostat is 29 °C and the stability is about 10 mK.

6. Results

Figure 4 shows the implementation of the PTB's and INRIM–POLITO's bridges in PTB's laboratory.

To check the consistency of the impedance bridges, two types of measurements were performed. The first type is the ratio measurement involving equal impedances $Z_1 \approx Z_2$: two 10 nF capacitors, two 12.9 kΩ resistors and one 12.9 kΩ resistor versus the ACQHR standard, all performed at 1233.15 Hz and 2466.3 Hz.

The second type is the quadrature measurement, involving a resistor and a capacitor in quadrature at a frequency for which $2\pi fRC \approx 1$. For this measurement type, a 10 nF capacitor is compared either with a 12.9 kΩ resistor or with the ACQHR, both performed at 1233.15 Hz, frequency of practical interest being close to both 1000 Hz and 1592 Hz (10 krad s^{-1}). These frequencies are the typical adopted values for the representation of the farad at national metrology institutes [45] and at the BIPM [46], and as mandatory frequencies in international intercomparisons [47].[5]

The impedance standards employed in the bridge assessment, introduced in sections 4 and 5, are listed in table 1.

Further, using the ratio measurement between 12.9 kΩ and R_{QHR}, and the two quadrature measurements between 10 nF and R_{QHR} as well as 12.9 kΩ and 10 nF, the triangle in figure 5 can be closed and the result should be zero in an ideal case. Any deviation from zero is a sign of unaccounted systematic effects.

The results of the comparison between the two bridges are reported in table 2.

The first and second columns report the measured quantity. The value of the working frequency f is reported in the third column for each configuration. The fourth and fifth columns report the results from the PTB Josephson impedance bridge and the INRIM–POLITO electronic digital bridge, respectively. These results are both corrected for the drifts of the temperature-controlled standards, according to the drift coefficients given in section 5. Finally, the column labeled δ reports the differences between the corresponding results. All

[5] The moderate frequency shift gives a very small capacitance change (at the level of 1×10^{-7} or lower) if performed on low-loss capacitors [48, 49].

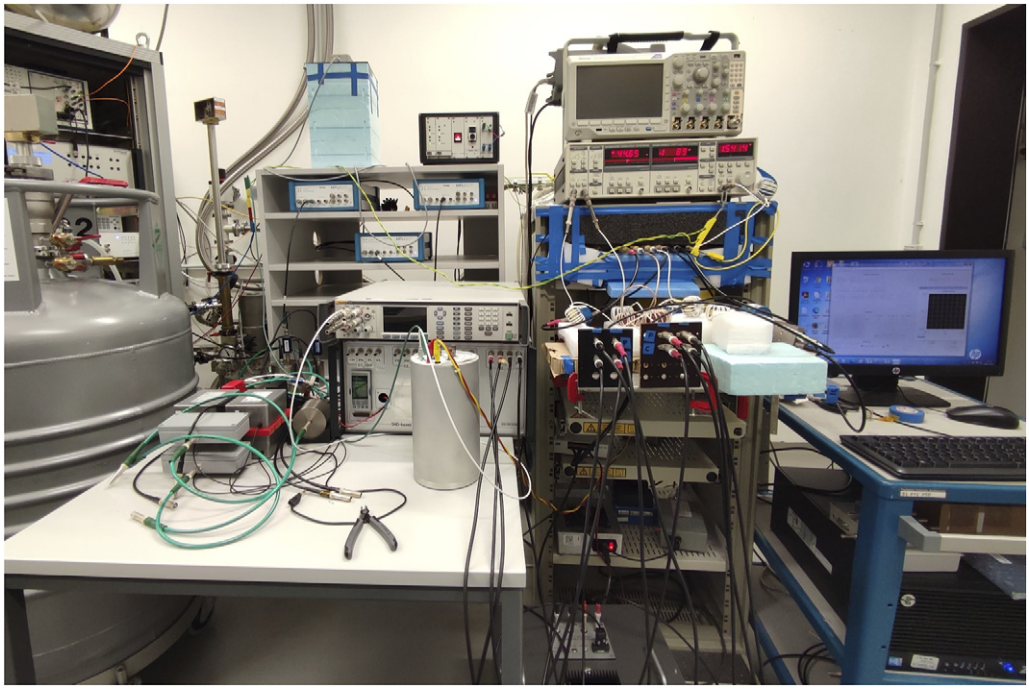

Figure 4. Implementation of the digital bridges developed by PTB (left) and INRIM–POLITO (right) in the PTB's laboratory.

Table 1. Impedance standards involved in the bridge assessment.

Name	Standard type	Value	Productor
R_1	Resistance	12.9 kΩ	PTB
R_2	Resistance	12.9 kΩ	INRIM
R_{QHR}	Resistance	ACQHR	PTB
C_1	Capacitance	10 nF	PTB
C_2	Capacitance	10 nF	PTB

the uncertainties are estimated separately for each bridge as described in detail in sections 2.3 and 3.4. They are reported with a coverage factor $k = 1$.

The last row reports the result of the triangle measurement performed among R_{QHR}, R_1 and C_2 at 1233 Hz as represented by the diagram in figure 5. The capacitance standard C_2 is first calibrated against R_1, which is in turn calibrated against the ACQHR standard R_{QHR}. Then, C_2 is directly calibrated against R_{QHR}. The results of the two calibrations of C_2 are then compared and the deviation of the combined ratios $(R_{\mathrm{QHR}}/R_1)(R_1C_2)/(R_{\mathrm{QHR}}C_2)$ from one is considered as a figure of merit.

The values of δ for each comparison are also shown in graphical form in figure 6. The uncertainty bars are drawn with the coverage factor $k = 1$. The blue band shows the 10^{-7} uncertainty level.

From the values of δ, all the measurements are compatible within the combined uncertainty with $k = 1$, except $C_1/C_2 - 1$ at 1233.15 Hz and $1/(2\pi f R_{\mathrm{QHR}}C_2) - 1$, which are compatible within the expanded uncertainty ($k = 2$). The uncertainty reported for the measurement $C_1/C_2 - 1$ at 2466.30 Hz performed by the INRIM–POLITO's bridge is greater than that of the other measurements because the current equalization was not yet well optimized as in the other configurations.

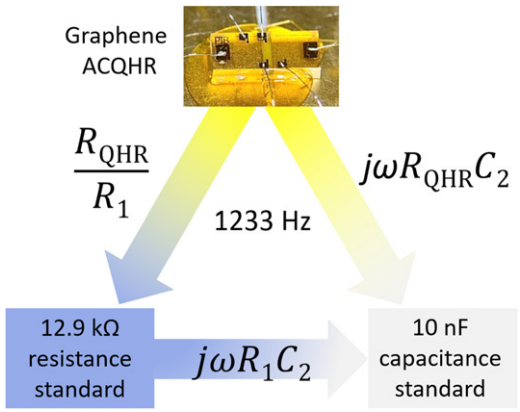

Figure 5. Diagram of the triangle measurement performed among R_{QHR}, R_1 and C_2 at 1233 Hz.

Some of the measurements were affected by larger temperature instability in the laboratory and in those cases the larger deviation between the two bridge measurements can be attributed to this. We can thus expect an even better compatibility in a temperature-controlled environment.

For the triangle measurements, the deviation measured with both impedance bridges is below four parts in 10^8 and for the INRIM–POLITO's bridge this can be assumed as zero within uncertainties. For the PTB's bridge, a deviation of two parts in 10^8 remains even when subtracting the uncertainties. This suggests unaccounted effects either in the ACQHR or in the bridge setup, especially for what concerns the cable correction and needs further investigation. However, the results obtained by both institutes agree well within the calculated combined uncertainties.

Table 2. Summary results of the comparison. All the uncertainties are reported with a coverage factor $k = 1$.

	Quantity	f/Hz	PTB	INRIM–POLITO	δ	Unit
A	$C_1/C_2 - 1$	1233.15	2.506(7)	2.731(111)	−0.225(114)	μF F^{-1}
B	$C_1/C_2 - 1$	2466.30	3.265(9)	3.292(221)	−0.027(221)	μF F^{-1}
C	$R_2/R_1 - 1$	1233.15	−21.633(9)	−21.564(102)	−0.069(103)	μΩ Ω^{-1}
D	$R_2/R_1 - 1$	2466.30	−21.808(11)	−21.772(108)	−0.036(109)	μΩ Ω^{-1}
E	$2\pi f R_1 C_1 - 1$	1233.15	10.311(9)	10.322(121)	−0.011(121)	μΩ Ω^{-1}
F	$R_{\mathrm{QHR}}/R_1 - 1$	1233.15	−7.734(9)	−7.773(102)	0.039(103)	μΩ Ω^{-1}
G	$1/(2\pi f R_{\mathrm{QHR}} C_2) - 1$	1233.15	0.266(9)	0.129(137)	0.137(116)	μΩ Ω^{-1}
H	$2\pi f R_1 C_2 - 1$	1233.15	7.504(9)	7.620(118)	−0.116(118)	μΩ Ω^{-1}
I	$(R_{\mathrm{QHR}}/R_1)(R_1 C_2)/(R_{\mathrm{QHR}} C_2) - 1$	1233.15	0.036(16)	0.024(194)	0.012(195)	μΩ Ω^{-1}

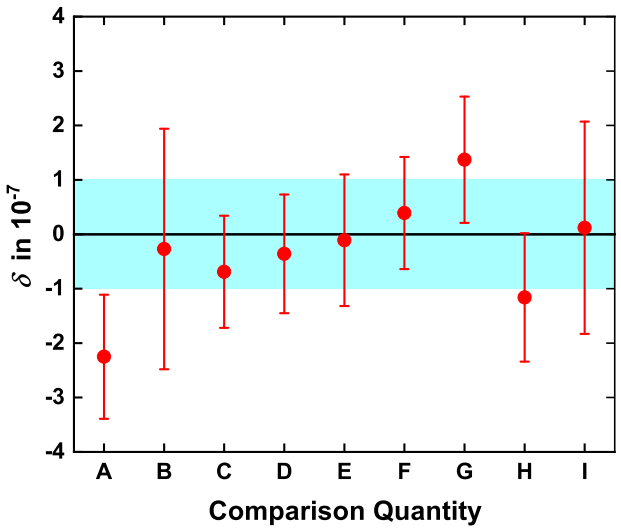

Figure 6. Values of δ according to table 2. The uncertainty bars are drawn with the coverage factor $k = 1$. The blue band shows the 10^{-7} uncertainty level.

The comparisons were thus performed at an uncertainty level comparable with that of top-level international capacitance intercomparisons [47].

7. Conclusions and outlook

We presented the results of a comparison performed at PTB between the digital bridges developed by PTB and INRIM–POLITO, based on Josephson and electronic waveform synthesizers, respectively. The useful onsite comparison was possible thanks to the easy transportability of the INRIM–POLITO's impedance bridge. Potentially, also the PTB's Josephson impedance bridge can be transported, but indeed it needs liquid helium to work. There is thus a significant advantage of digital bridges beyond their measurement capabilities. The comparison was performed with both like ($R:R$ and $C:C$) and quadrature ($R:C$) impedances at 1 : 1 magnitude ratio. This choice of the magnitude ratio was necessary to achieve an optimal and competitive uncertainty with the INRIM–POLITO's electronic digital bridge. The working frequencies were chosen to be close to the values typically adopted for the representation of the farad in international intercomparisons [47].

The comparison showed good compatibility between the results obtained with the two impedance bridges. The resulted uncertainty level is comparable with that of top-level international capacitance intercomparisons.

The Josephson bridge has indeed an uncertainty which is an order of magnitude less than that of the electronic bridge, and can operate with the lowest uncertainty over a wide range of impedance ratios. The electronic digital bridge is an affordable impedance bridge capable of calibrating like and quadrature impedance standards, including ACQHR standards, in the 1 : 1 magnitude ratio with an uncertainty of about one part in 10^7 ($k = 1$), suitable for primary impedance metrology.

A realization uncertainty of the farad unit at the level of one part in 10^7 can endorse a calibration activity of artifact capacitance standards and meters with uncertainties comparable with those of the best presently available calibration services [46].

The comparison scheme makes δ independent of a possible apparent frequency dependence of the Hall resistance. The frequency dependence of optimized graphene devices is expected to be smaller than in traditional GaAs ones [50] and will be the focus of future studies.

Further comparisons can be undertaken by measuring the same impedance standards and QHR sample at different institutes.

Acknowledgments

This Project 18SIB07 GIQS—*Graphene Impedance Quantum Standard* has received funding from the EMPIR programme co-financed by the Participating States and from the European Unions' Horizon 2020 research and innovation programme. Martina Marzano received funding from the EMPIR Research Mobility Grant 18SIB07-RMG1 related to the Joint Research Project GIQS. We also thank Jürgen Schurr and Martin Götz for helping with the calibration of the impedances and Oliver Kieler and his team for providing the JAWS arrays. The comparison was undertaken in the framework of the EURAMET TCEM project n. 1501: "Technical assessment of novel digital impedance bridges".

ORCID iDs

Martina Marzano https://orcid.org/0000-0001-5288-3093
Yaowaret Pimsut https://orcid.org/0000-0001-9210-6512
Mattias Kruskopf https://orcid.org/0000-0003-2846-3157
Marco Kraus https://orcid.org/0000-0002-7592-9493
Vincenzo D'Elia https://orcid.org/0000-0001-6924-0430

Luca Callegaro https://orcid.org/0000-0001-5997-9960
Massimo Ortolano https://orcid.org/0000-0002-7217-8276
Stephan Bauer https://orcid.org/0000-0001-6242-2223
Ralf Behr https://orcid.org/0000-0002-5480-443X

References

[1] Bureau International des Poids et Mesures 2019 *SI Brochure* https://www.bipm.org/utils/common/pdf/si-brochure/SI-Brochure-9-EN.pdf
[2] Göbel E O and Siegner U 2019 *The New International System of Units (SI): Quantum Metrology and Quantum Standards* (New York: Wiley)
[3] Poirier W, Djordjevic S, Schopfer F and Thévenot O 2019 The ampere and the electrical units in the quantum era *C. R. Phys.* **20** 92–128
[4] Rigosi A F and Elmquist R E 2019 The quantum Hall effect in the era of the new SI *Semicond. Sci. Technol.* **34** 093004
[5] Gibbings D L H 1963 A design for resistors of calculable a.c./d.c. resistance ratio *Proc. Inst. Electr. Eng. UK* **110** 335–47
[6] Boháček J and Wood B M 2001 Octofilar resistors with calculable frequency dependence *Metrologia* **38** 241
[7] Haddad R J 1969 A resistor calculable from DC to $\omega = 10^5$ rad s^{-1} M. S. Thesis Sch. Eng. Appl. Sci., George Washington Univ.
[8] Awan S, Kibble B and Schurr J 2011 *Coaxial Electrical Circuits for Interference-free Measurements Coaxial Electrical Circuits for Interference-free Measurements* (London: The Institution of Engineering and Technology)
[9] Callegaro L 2013 *Electrical Impedance: Principles, Measurement, and Applications Series in Sensors* (Boca Raton, FL: CRC Press)
[10] Schurr J, Bürkel V and Kibble B P 2009 Realizing the farad from two ac quantum Hall resistances *Metrologia* **46** 619
[11] Overney F and Jeanneret B 2011 RLC bridge based on an automated synchronous sampling system *IEEE Trans. Instrum. Meas.* **60** 2393–8
[12] Callegaro L, D'Elia V, Kampik M, Kim D B, Ortolano M and Pourdanesh F 2015 Experiences with a two-terminal-pair digital impedance bridge *IEEE Trans. Instrum. Meas.* **64** 1460–5
[13] Kürten Ihlenfeld W G and Vasconcellos R T B 2016 A digital four terminal-pair impedance bridge *2016 Conf. Precis. Electromagn. Meas. (CPEM 2016)* vol 7 (Ottawa, Canada: IEEE) pp 1–2
[14] Overney F, Flowers-Jacobs N E, Jeanneret B, Rüfenacht A, Fox A E, Underwood J M, Koffman A D and Benz S P 2016 Josephson-based full digital bridge for high-accuracy impedance comparisons *Metrologia* **53** 1045
[15] Bauer S, Behr R, Hagen T, Kieler O, Lee J, Palafox L and Schurr J 2017 A novel two-terminal-pair pulse-driven Josephson impedance bridge linking a 10 nF capacitance standard to the quantized Hall resistance *Metrologia* **54** 152
[16] Hagen T, Palafox L and Behr R 2017 A Josephson impedance bridge based on programmable Josephson voltage standards *IEEE Trans. Instrum. Meas.* **66** 1539–45
[17] Kucera J and Kovac J 2018 A reconfigurable four terminal-pair digitally assisted and fully digital impedance ratio bridge *IEEE Trans. Instrum. Meas.* **67** 1199–206
[18] Overney F and Jeanneret B 2018 Impedance bridges: from Wheatstone to Josephson *Metrologia* **55** S119
[19] Ortolano M, Palafox L, Kučera J, Callegaro L, D'Elia V, Marzano M, Overney F and Gülmez G 2018 An international comparison of phase angle standards between the novel impedance bridges of CMI, INRIM and METAS *Metrologia* **55** 499–512
[20] Overney F, Flowers-Jacobs N E, Jeanneret B, Rüfenacht A, Fox A E, Dresselhaus P D and Benz S 2020 Dual Josephson impedance bridge: towards a universal bridge for impedance metrology *Metrologia* **57** 065014
[21] Marzano M, Ortolano M, D'Elia V, Müller A and Callegaro L 2020 A fully digital bridge towards the realization of the farad from the quantum Hall effect *Metrologia* **58** 015002
[22] Bauer S *et al* 2021 A four-terminal-pair Josephson impedance bridge combined with a graphene-quantized Hall resistance *Meas. Sci. Technol.* **32** 065007
[23] Kalmbach C-C, Schurr J, Ahlers F J, Müller A, Novikov S, Lebedeva N and Satrapinski A 2014 Towards a graphene-based quantum impedance standard *Appl. Phys. Lett.* **105** 073511
[24] Ribeiro-Palau R *et al* 2015 Quantum Hall resistance standard in graphene devices under relaxed experimental conditions *Nat. Nanotechnol.* **10** 965–71
[25] Lafont F *et al* 2015 Quantum Hall resistance standards from graphene grown by chemical vapour deposition on silicon carbide *Nat. Commun.* **6** 6806
[26] Rigosi A F *et al* 2019 Graphene devices for tabletop and high-current quantized Hall resistance standards *IEEE Trans. Instrum. Meas.* **68** 1870–8
[27] Kruskopf M and Elmquist R E 2018 Epitaxial graphene for quantum resistance metrology *Metrologia* **55** R27
[28] GIQS—graphene impedance quantum standard— 2019 *EMPIR 18SIB07*
[29] Marzano M, Pimsut Y, Kruskopf M, Kraus M, Ortolano M, Bauer S, Behr R and Callegaro L 2022 Novel digital impedance bridges for the realization of the farad from graphene quantum standards *2022 3rd URSI Atlantic and Asia Pacific Radio Science Meeting (AT-AP-RASC)* (IEEE)
[30] Cutkosky R D 1964 Four-terminal-pair networks as precision admittance and impedance standards *IEEE Trans. Commun. Electron.* **83** 19–22
[31] Delahaye F 1993 Series and parallel connection of multiterminal quantum Hall-effect devices *J. Appl. Phys.* **73** 7914–20
[32] Schurr J, Moser H, Pierz K, Ramm G and Kibble B P 2011 Johnson–Nyquist noise of the quantized Hall resistance *IEEE Trans. Instrum. Meas.* **60** 2280–5
[33] Burroughs C J, Benz S P and Dresselhaus P D 2003 AC Josephson voltage standard error measurements and analysis *IEEE Trans. Instrum. Meas.* **52** 542–4
[34] Landim R P, Benz S P, Dresselhaus P D and Burroughs C J 2008 Systematic-error signals in the AC Josephson voltage standard: measurement and reduction *IEEE Trans. Instrum. Meas.* **57** 1215–20
[35] Underwood J M 2019 Uncertainty analysis for ac–dc difference measurements with the AC Josephson voltage standard *Metrologia* **56** 015012
[36] Marzano M, Tran N T M, D'Elia V, Serazio D, Enrico E, Ortolano M, Pierz K, Kucera J and Callegaro L 2021 Design and development of a coaxial cryogenic probe for precision measurements of the quantum Hall effect in the AC regime *Acta IMEKO* **10** 24–9
[37] Kaczmarek J, Rybski R and Kozioł M 2016 The polyphase ac voltage source for digital impedance bridges *Final Dissemination Workshop of EMRP Projects AIM QuTE, GraphOhm and Q-WAVE* https://ptb.de/emrp/sib53-finalworkshop.html
[38] Ortolano M *et al* 2020 Error sources in electronic fully-digital impedance bridges *2020 Conf. Precis. Electromagn. Meas. (CPEM 2020)* pp 1–2
[39] Sutton C M and Clarkson M T 1994 A general approach to comparisons in the presence of drift *Metrologia* **30** 487
[40] Swanson H E and Schlamminger S 2010 Removal of zero-point drift from AB data and the statistical cost *Meas. Sci. Technol.* **21** 115104

[41] Ortolano M *et al* 2021 A comprehensive analysis of error sources in electronic fully digital impedance bridges *IEEE Trans. Instrum. Meas.* **70** 1500914
[42] Chae D-H *et al* 2022 Investigation of the stability of graphene devices for quantum resistance metrology at direct and alternating current *Meas. Sci. Technol.* **33** 065012
[43] Kruskopf M *et al* 2021 Graphene quantum Hall effect devices for AC and DC electrical metrology *IEEE Trans. Electron Devices* **68** 3672–7
[44] Schurr J, Kibble B P, Hein G and Pierz K 2009 Controlling losses with gates and shields to perfect a quantum Hall impedance standard *IEEE Trans. Instrum. Meas.* **58** 973–9
[45] Koffman A, Wang Y and Shields S 2007 NIST measurement services: three-terminal precision standard capacitor calibrations at NIST NIST, Tech. Rep. NIST SP 250-76
[46] Bureau International des Poids et Mesures 2021 Technical service—calibration of capacitance standards https://bipm.org/en/electrical-metrology/calibrations
[47] Consultative Committee for Electricity and Magnetism 2019 CCEM–K4.2017: comparison of 10 pF capacitance standards https://bipm.org/kcdb/comparison?id=444
[48] Wang Y 2003 Frequency dependence of capacitance standards *Rev. Sci. Instrum.* **74** 4212–5
[49] Callegaro L and Sellone M 2016 The frequency dependence of a 10 nF gas-dielectric capacitor *2016 Conf. Precision Electromagnetic Measurements (CPEM 2016)* (IEEE)
[50] Luond F, Kalmbach C-C, Overney F, Schurr J, Jeanneret B, Muller A, Kruskopf M, Pierz K and Ahlers F 2017 AC quantum Hall effect in epitaxial graphene *IEEE Trans. Instrum. Meas.* **66** 1459–66